Cloud Condensation Nuclei Activity of $CaCO_3$ Particles with Oleic Acid and Malonic Acid Coatings

Mingjin Wang[1,2], Tong Zhu[1*], Defeng Zhao[2], Florian Rubach[2,3], Andreas Wahner[2], Astrid Kiendler-Scharr[2], and Thomas F. Mentel[2*]

[1]BIC-ESAT and SKL-ESPCl, College of Environmental Sciences and Engineering, Peking University, Beijing 100871, China.

[2]Institut für Energie- and Klimaforschung (IEK-8), Forschungszentrum Jülich GmbH, 52425 Jülich, Germany.

[3]Klimageochemie, Max Planck Institut für Chemie, 55128 Mainz, Germany

[*] To whom correspondence should be addressed: tzhu@pku.edu.cn; t.mentel@fz-juelich.de

Abstract.

Condensation of carboxylic acids on mineral particles will lead to coatings, and impact on the particles' potential to act as cloud condensation nuclei (CCN). To determine how the CCN activity of mineral particles is impacted by carboxylic acid coatings, the CCN activity of $CaCO_3$ particles and $CaCO_3$ particles with oleic acid and malonic acid coatings were compared in this study. The results revealed that small

amounts of oleic acid coating (volume fraction (vf) ≤ 4.3%) decreased the CCN activity of $CaCO_3$ particles, while more oleic acid coating (vf ≥16%) increased the CCN activity of $CaCO_3$ particles. This phenomenon has not been reported before. On the other hand, the CCN activity of $CaCO_3$ particles coated with malonic acid increased with the thickness of the malonic acid coating (vf = 0.4 - 40%). Even smallest amounts of malonic acid coating (vf = 0.4%) significantly enhanced the CCN activity of $CaCO_3$ particles from $\kappa = 0.0028 \pm 0.0001$ to $\kappa = 0.0123 \pm 0.0005$. This supports that a small amount of water-soluble organic acid coating may significantly enhance the CCN activity of mineral particles. The presence of water vapor during the coating process with malonic acid additionally increased the CCN activity of the coated $CaCO_3$ particles, probably because more $CaCO_3$ reacts with malonic acid if sufficient water is available.

1 Introduction

Atmospheric aerosols serve as cloud condensation nuclei and change the radiative properties (cloud albedo effect) and lifetime (cloud lifetime effect) of clouds, thus affecting the Earth's climate indirectly (Liu and Wang, 2010; Gantt et al., 2012; Penner et al., 2004; Haywood and Boucher, 2000). Mineral aerosol is one of the most abundant components of the atmospheric aerosol. It is estimated that 1500-2600 Tg of mineral aerosol particles with radii between 0.1 and 8 μm are emitted annually into the atmosphere on a global scale (Cakmur et al., 2006). Mineral aerosol particles are mainly composed of substances that are slightly soluble or insoluble in water. Cloud condensation nuclei (CCN) activity measurements show that the hygroscopicity parameter κ (Petters and Kreidenweis, 2007) varies between 0.001 and 0.08 for mineral aerosols, including $CaCO_3$ aerosol, clay aerosols and mineral dust aerosols generated in the laboratory or sampled from various locations worldwide (Garimella et al., 2014; Yamashita et al., 2011; Zhao et al., 2010; Koehler et al., 2009; Sullivan et al., 2010; Herich et al., 2009). The low κ indicates that the CCN activity of mineral aerosol is much lower than the CCN activity of water soluble salts like $(NH_4)_2SO_4$ (κ = 0.61) and NaCl (κ = 1.28), which are also common in atmospheric aerosols (Petters and Kreidenweis, 2007). Tang et al. (2016) reviewed recently the interaction of mineral dust particles with water.

Mineral aerosol particles can be coated by organic vapors during their residence and transport in the atmosphere. Many individual particle measurements have shown that mineral components and organic matter can coexist in the same individual aerosol

particle in the real atmosphere (Falkovich et al., 2004; Falkovich et al., 2001; Russell et al., 2002; Li and Shao, 2010). Carboxylic acids (R(C=O)OH) are abundant species among the organic matter that coexists with mineral particles. Russell et al. (2002) found that carbonyls (R(C=O)R), alkanes, and R(C=O)OH are present in individual mineral (and sea salt) aerosol particles, with enhanced concentration of R(C=O)OH. They also found that Ca^{2+}, CO_3^{2-}, R(C=O)OH and R(C=O)R coexisted in some individual mineral aerosol particles with a strong correlation between CO_3^{2-} and R(C=O)OH. These particles could be formed by $CaCO_3$ particles (partly) coated with organic film. Falkovich et al. (2004) also found that organic and inorganic components coexisted in individual mineral aerosol particles with the organic component consisting of various short-chain (C_1-C_{10}) mono- and dicarboxylic acids (MCA and DCA). The concentration of short-chain carboxylic acids in mineral aerosol particles increased with the increase of the ambient relative humidity. A possible explanation for such observations could be that when more water is condensed onto mineral particles at higher ambient relative humidity, the adsorbed carboxylic acids are ionized in the aqueous environment and react with mineral particles forming organic acid salts. Of the major components of mineral aerosol particles (clay, calcite ($CaCO_3$), quartz, mica, feldspar, etc.), only $CaCO_3$ with alkaline character can react with carboxylic acids in this way. Thus $CaCO_3$ may play a key role in the uptake of carboxylic acids by mineral aerosol particles.

Carboxylic acid coatings on mineral aerosol particles change their chemical composition and thus may have an impact on their CCN activity. Many previous studies have investigated the CCN activity of pure mineral aerosol (Garimella et al., 2014; Yamashita et al., 2011; Zhao et al., 2010; Koehler et al., 2009; Sullivan et al., 2010; Herich et al., 2009) and pure carboxylic acid aerosol (Kumar et al., 2003; Hori

et al., 2003; Cruz and Pandis, 1997; Hartz et al., 2006), but only a few studies have investigated the CCN activity of mineral aerosol particles with carboxylic acid coatings (Tang et al., 2015; Hatch et al., 2008; Gierlus et al., 2012).

In this study we used malonic acid and oleic acid as coating materials and $CaCO_3$ particles as cores, and investigated the CCN activity of the coated $CaCO_3$ particles. Herein we varied the coating thickness and the relative humidity during the coating process. Malonic acid is a representative of the class of dicarboxylic acids and oleic acid is an example of surfactant like compounds. Dicarboxylic acids are ubiquitous in the atmosphere (Kawamura et al., 1996; Kawamura and Ikushima, 1993; Ho et al., 2007; Mkoma and Kawamura, 2013; Kawamura and Bikkina, 2016) and formed by photochemical reactions and ozonolysis (Chebbi and Carlier 1996; Kawamura and Bikkina, 2016; Kawamura et al., 1996; Khare et al. 1999; Mellouki et al., 2015). It has been reported that dicarboxylic acids (C_2-C_{10}) account for 0.06-1.1% of the total aerosol mass, with higher values in the summer, and 1.8% of the total aerosol carbon (TC) in urban aerosol, in which oxalic acid, malonic acid, and succinic acid are the most abundant species (Kawamura et al., 1996; Kawamura and Ikushima, 1993; Ho et al., 2007; Mkoma and Kawamura, 2013). Oleic acid, which is emitted into the atmosphere by the cooking of meat, wood burning, and automobile source (Schauer et al., 1999; Rogge et al., 1998; Rogge et al., 1993), is present in atmospheric aerosols of urban, rural, and forest areas (Cheng et al., 2004; Ho et al., 2010). The water solubility of the two organic acids is complementary; it is high for malonic acid while it is very low for oleic acid. Coatings of malonic acid and oleic acid could thus have different effects on CCN activity of mineral particles.

2 Experimental

As general procedure, $CaCO_3$ aerosol was generated according to Zhao et al. (2010), and then poly- or monodisperse $CaCO_3$ aerosol particles were coated by malonic or oleic acid in a coating device. A flow tube was optionally applied to extend the residence time. The particle size, chemical composition, and CCN activity of the $CaCO_3$ particles were measured before and after coating. Figure 1 shows the schematic of the experimental set up.

2.1 Generation of $CaCO_3$ aerosol

$CaCO_3$ aerosol was generated by spraying a saturated $Ca(HCO_3)_2$ solution. A sample of $CaCO_3$ powder (2 g, pro analysis, ≥99%, Merck, Darmstadt, Germany) was suspended in 1-L Milli-Q water (18.2 MΩcm, TOC <5 ppb). Then about 1.5 L min^{-1} CO_2 (purity ≥99.995%, Praxair Industriegase GmbH & Co. KG, Magdeburg, Germany) was bubbled into the suspension at room temperature for 3 h, while the suspension was stirred using a magnetic stirrer. During bubbling, CO_2 reacted with $CaCO_3$ to produce $Ca(HCO_3)_2$. After bubbling, the suspension was allowed to settle for 10 min, the supernatant clear $Ca(HCO_3)_2$ solution was decanted and used for spraying by a constant output atomizer (Model 3076, TSI, Shoreview, MN, USA) using 1.75 L min^{-1} high-purity N_2 (Linde LiPur 6.0, purity 99.9999%, Linde AG, Munich, Germany).

125 The major portion (0.9 L min^{-1}) of the aerosol flow generated by spraying was dried
126 in a diffusion drier filled with silica gel. The relative humidity was below 10% after
127 drying. The remainder of the aerosol flow was drawn off by a pump and discarded.
128 The dry aerosol was passed through a tube furnace (Model RS 120/1000/12,
129 Nabertherm GmbH, Lilienthal, Germany) set at 300 ºC. The residence time of the
130 aerosol in the furnace was 5.2 s. Zhao et al. (2010) described this method for
131 generating $CaCO_3$ aerosol in detail. At room temperature dry $Ca(HCO_3)_2$ is
132 thermodynamically unstable and decays into $CaCO_3$, CO_2, and H_2O (Keiser and
133 Leavitt, 1908). With this method the aerosol still contained some $Ca(HCO_3)_2$ after
134 drying, but after heating at 300 ºC it was completely converted into $CaCO_3$ (Zhao et
135 al., 2010). The $CaCO_3$ aerosol generated was either first size selected by a Differential
136 Mobility Analyzer (DMA, TSI 3081) with a neutralizer on the inlet or entered the
137 coating device directly as poly-disperse aerosol.

138 Figure 2 (upper panel) shows the total number concentration and mean size of the
139 bare $CaCO_3$ aerosol particles generated at different spraying time, which were
140 measured with the SMPS described below. The mean size (mode diameter) stabilized
141 after about 50 min in the range 49.8-55.5 nm. Over the 232 min spraying time, the
142 total number concentration varied in the range 1.8×10^6–4.5×10^6 cm^{-3}. The total
143 number concentration decreased by about 1/3 in the initial 70 min. The decrease
144 became slower after 70 min and the total number concentration tended to stabilize
145 after 155 min. After 70 min the total number concentration varied in a smaller range
146 of 1.8×10^6–2.9×10^6 cm^{-3}, therefore, the measurements in this study typically started

147 after 70 min spraying. The typical size distribution of the $CaCO_3$ aerosol particles
148 after 70 min spraying is shown in Fig. 2 (lower panel). The $CaCO_3$ particles showed a
149 single mode distribution with a mode diameter at 32.2 nm. The number concentration
150 was more than 100 cm^{-3} for particles between 9.82 and 346 nm.

151 **2.2 Organic acid coating**

152 The coating device (Fig. 1, right hand side) used in this study was designed by Roselli
153 (2006), and showed good reproducibility, controllability, and stability. The glass
154 apparatus consisted of a small storage bulb (100 ml) holding the organic coating
155 substances which was directly connected to a mixing cell (about 35 ml). The storage
156 bulb and mixing cell were fully immersed in a flow-through water heater connected to
157 a thermostatic bath (F25, Julabo GmbH, Seelbach, Germany). The temperature range
158 of the thermostatic bath used in this study was 30-80 ºC. An extra N_2 stream could be
159 passed through the storage bulb in order to enhance the organic vapors flowing into
160 the mixing cell. The outflow of the coating device was connected to a Liebig type
161 water cooler. The water cooler was controlled by another thermostatic bath (F25,
162 Julabo GmbH, Seelbach, Germany) operated at 25 ºC throughout all of the
163 experiments.

164 The bottom of the storage bulb was filled with either 5.0 g malonic acid powder
165 (assay ≥98%(T), Fluka Chemika, Sigma-Aldrich, St Louis, MO, USA) or 10.0 ml
166 oleic acid (chemical purity (GC) 99.5%, Alfa Aesar, Ward Hill, MA, USA). A flow of
167 0.9 L min^{-1} high purity N_2 was used to carry the organic acid vapor up into the mixing
168 cell. The flow of 0.9 L min^{-1} $CaCO_3$ aerosol was passed through the mixing cell and
169 mixed with the 0.9 L min^{-1} N_2 flow carrying the organic acid vapor. The mixed flow

then entered the water cooler. The organic acid vapor was condensed on $CaCO_3$ aerosol particles in both the mixing cell and the water cooler. The residence time of the aerosol in the coating device including the cooler was about 6 seconds Three identical coating devices, with the same heating and cooling thermostatic bath, were used: one for malonic acid coating, one for oleic acid coating, and a blank one without organic acid for assessing the impact caused by heating the $CaCO_3$ aerosol in the coating device without organic acid (Roselli, 2006).

The aerosol could enter the measuring instruments directly, or after passing through a flow tube to increase its residence time. The flow tube was made of a straight circular glass tube with a 2.5 cm internal diameter. The aerosol flow in the flow tube was laminar flow. The residence time of the aerosol in the flow tube was 23.7 s.

For the coating process we mixed flows of 0.9 L min^{-1} of dry N_2 and of aerosol dried to <10% relative humidity (RH) at room temperature (RT). As a consequence RH at the outlet of the coating device was <5% at RT. To investigate the impact of water on the coating process and CCN activity, organic coating at a higher relative humidity was also performed. For that a bubbling device filled with Milli-Q water was utilized to saturate the N_2 stream with water vapor before it entered the storage bulb (RH>90% at RT). After mixing with the aerosol stream at RH ≈10%, the water concentration in the mixing cell corresponded to RH ≈ 50% at RT or a partial pressure of ≈1500 Pa. The relative humidity of the aerosol at the outlet of the coating device at RT was indeed ~47% when humidification was applied. For the partial water vapor pressure of 1500 Pa we calculated RH >7% at 60°C (for MA), and RH >3% at 80°C (for OA) which is about an order of magnitude higher than RH in the dry cases. In fact RH will be somewhat higher as the gas-phase may not reach the bath temperature which

primarily serves to warm up the coating agent and control its vapor pressure.

2.3 Size and chemical composition measurements

The number size distribution of the aerosol particles was measured using a Scanning Mobility Particle Sizer (SMPS, TSI 3080 Electrostatic Classifier with TSI 3081 DMA, TSI 3786 UWCPC). The sample flow was set to 0.6 L min^{-1} and the sheath flow was set to 6.0 L min^{-1}. The size range measured was 9.82-414.2 nm with a size resolution of 64 channels per decade and the time resolution was 3 min for a complete scan. Despite the maximum resolution of the SMPS the size bin width was still substantial compared to the observed growth by coating. We therefore derived the diameter of the coated (and the respective bare $CaCO_3$ particles) by interpolating in between the size bins. For that we considered 5-9 size bins around the size bin of nominal mode and fitted a lognormal distribution to these data. The fitted mode positions are listed in Table 1. The error bars in x direction in Figure S1 in the supplement, show the shifts of the fitted mode position relative to the nominal size bin.

The chemical composition and the vacuum aerodynamic diameter of the aerosol particles were measured using a High-Resolution Time-of-Flight Aerosol Mass Spectrometer (HR-ToF-AMS, Aerodyne Research Inc., Billerica, MA, USA (DeCarlo et al., 2006)). The aerosol particles were vaporized at 600 ºC and ionized by electron impact ionization at 70 eV, i.e. we focused on the measurements of the organic coatings and sacrificed a direct $CaCO_3$ determination by AMS (compare Zhao et al. 2010). The AMS was routinely operated in V-mode in two alternating modes: 1 min MS mode to measure the chemical composition and 2 min PToF mode. Only MS mode data were analyzed. AMS measurements and SMPS measurements were synchronous and both were repeated at least four times for each sample. Size

information for bare $CaCO_3$ was taken from SMPS data in the blank coating device.

We used specific marker *m/z* to derive the amount of organic coating. For pure oleic acid the signal at *m/z*41 ($C_3H_5^+$) was reported to be the strongest signal in the mass spectrum measured by Q-AMS at EI energy of 70 eV and vaporizer temperature of 600 ºC (Sage et al., 2009). The signal at *m/z*41 was also strongest for oleic acid coatings in our HR mass spectra. In order to get a high signal to noise ratio we choose the signal at *m/z*41 in the MS mode of the AMS measurement as a marker for oleic acid in the coated $CaCO_3$ particles. There was no significant signal at *m/z*41 for the uncoated $CaCO_3$ particles. The average background signal at *m/z*41 per single aerosol particle corresponded to $2.4\pm0.79\cdot10^{-12}$ µg for bare $CaCO_3$. The average value presented the baseline of the mass spectra and the standard deviation was derived from the noise of the mass spectra at *m/z*41. Similarly, the signal at *m/z*42 ($C_2H_2O^+$) was one of the strongest signals in the mass spectrum of pure malonic particles measured by Q-AMS with EI energy of 70 eV and vaporizer temperature of 600 ºC (Takegawa et al., 2007). That signal was also observed for malonic acid coatings in our HR mass spectra and used as marker for malonic acid coatings. The average background signal per aerosol particle at *m/z42* for bare $CaCO_3$ particles was $1.4\pm0.42\cdot10^{-12}$µg. The average value represented the baseline of the mass spectra at *m/z*42 and the standard deviation was derived from the noise in the mass spectra.

The coating amount for both organic compounds was derived as follows. The observed signal at the respective marker *m/z* was corrected for the background signal from bare $CaCO_3$ and then scaled to the volume increase (per particle) calculated from the shift of the particle diameter D_P for the largest coating amount achieved at 80 ºC coating temperature. Because of the relative large bin width compared to the

growth by coating we used the D_P's, interpolated between the nominal size bins of the SMPS (see above). This assumed spherical core shell morphology, based on Zhao et al. (2011) where we showed that the $CaCO_3$ particles generated by our spray drying method are spherical. The relation between AMS derived organic mass (baseline corrected marker signals at *m/z41* or *m/z42* per particle) and SMPS derived organic mass ($\pi/6 \cdot (D_P)^3/\rho_{org}$) is linear within the limits of the method (see Figure S1 in the supplement). For discussion we will refer to the AMS results, as we are able to detect amounts of organic coatings as small as few time 10^{-12} ug per particle with the AMS, while these could be not be detected by the SPMS.

2.4 CCN activity measurement

The aerosol was dried to RH <3% by another diffusion drier before the CCN activity was measured. To determine the CCN activity of the aerosol, the number concentration of the cloud condensation nuclei (CCN) of the aerosol was measured with a continuous flow CCN counter (CCNC, DMT-100, Droplet Measurement Technologies, Boulder, CO, USA). The total number concentration (CN) of the aerosol particles was synchronously measured using an ultrafine water-based condensation particle counter (UWCPC, TSI 3786, cf. Zhao et al., 2010). The ratio of CCN to CN (CCN/CN) is called the activated fraction (a_f). In cases where poly-disperse aerosol was coated, the coated aerosol particles were size selected by scanning a DMA between 10.6 and 478.3 nm , and the CCN and CN concentrations were determined for each size bin while the super-saturation (SS) kept constant (known as 'Scanning Mobility CCN Analysis (SMCA)', Moore et al., 2010). The activated fraction was calculated after the CCN and CN concentrations were corrected for the multiple charged particles.

The activated fraction as a function of the particle size was fitted with a cumulative Gaussian distribution function (Rose et al., 2008). The turning point of the function is the critical dry diameter (D_{crit} or D_{50}) at the set SS. The activation efficiency (i.e., the activated fraction when aerosol particles are completely activated) was 83% for the CCN instrument, determined using 150 nm $(NH_4)_2SO_4$ particles at SS=0.85%. Besides $CaCO_3$ and coated $CaCO_3$ particles, the CCN activity of malonic acid particles, oleic acid particles, and mixed particles of $CaCO_3$ and malonic acid was also measured. The oleic acid particles were generated by heating 10.0 ml oleic acid to 97 ºC in the storage bulb and then cooling the vapor to 2 ºC in the water cooler in a clean coating device. 1.75 L min^{-1} high-purity N_2 was used as carrying gas and went into the storage bulb through‘1 N_2 in‘ entrance in Fig. 1; the‘3 Aerosol in‘ entrance in Fig. 1 was closed. This way, pure oleic acid particles with diameters up to 333 nm were generated. Mixed $CaCO_3$/malonic acid particles were generated by spraying the supernatant clear solutions which were prepared by settling suspensions containing $CaCO_3$ and malonic acid in molar ratios of about 1:1 and 3:1. The suspensions were prepared with 0.020 g malonic acid and 0.021 g $CaCO_3$ and 0.025 g malonic acid and 0.076 g $CaCO_3$ in 1000 ml Milli-Q water, respectively. The suspensions were allowed to stand for 24h.

For aerosols where monodisperse aerosol particles with a dry diameter D_P were coated, the CCN concentration was measured at different SS and the CN concentration was measured synchronously. Similarly, the activated fraction as a function of SS was fitted with a sigmoidal function. The turning point of the function is the critical supersaturation (SS_{crit}) and the corresponding to the dry diameter D_P is also called the critical diameter, D_{crit}. The hygroscopicity parameter κ (Petters and Kreidenweis, 2007) was then calculated from the $D_P(D_{crit})$-SS_{crit} or $SS(SS_{crit})$-D_{crit} data

set. The SS settings of the CCN counter were calibrated weekly using $(NH_4)_2SO_4$ aerosol based on the theoretic values in the literature (summarized by Rose et al., 2008).

3 Results and discussion

3.1 CCN activity of $CaCO_3$ aerosol

Before the coating experiments we determined the CCN activity of the bare $CaCO_3$ aerosol particles. It was measured by the scanning method (SMCA) using poly-disperse $CaCO_3$ aerosol particles. The value of the hygroscopicity parameter κ of the $CaCO_3$ aerosol was 0.0028 ± 0.0001 derived by the least-square-fitting of D_{crit} as a function of SS (SS_{crit}). This κ value is quite small, indicating that the CCN activity of the $CaCO_3$ aerosol is low. Our κ is well within the range of κ's of 0.0011 ± 0.0004 to 0.0070 ± 0.0017 found in previous studies for wet generated $CaCO_3$ particles (Zhao et al., 2010; Sullivan et al., 2009; Gierlus et al., 2012, Tang et al., 2016), but larger than κ for dry generated $CaCO_3$ aerosols (0.008-0.0018, Sullivan et al., 2009).

The CCN activity for $CaCO_3$ aerosol passed through the blank coating device and exposed to temperatures of 60 ºC and 80 ºC was determined using the same method. The κ value remained 0.0028 ± 0.0001 up to 60 ºC and increased to 0.0036 ± 0.0001 at 80 ºC. The increased κ value of 0.0008 at 80 ºC was lower than the differences of reported κ values for $CaCO_3$ aerosol in various studies, and much lower than the changes of κ values measured in this study when the $CaCO_3$ aerosol particles were coated by malonic or oleic acid. So the effect of heating the $CaCO_3$ aerosol during the

312 coating process on the CCN activity of the $CaCO_3$ aerosol was neglected. The D_{crit} at
313 different supersaturations (SS_{crit}) for the $CaCO_3$ aerosol and for the $CaCO_3$ aerosol
314 passed through a blank coating device at heating temperatures of 60 ºC and 80 ºC are
315 shown in Fig. 5 (red, yellow and green circles).

316 As the solubility of $CaCO_3$ in water is very low, droplet activation of $CaCO_3$ (and
317 other mineral dust components) is often described by a water adsorption approach,
318 wherein the solute term B in the Köhler equation (Köhler 1936, Seinfeld and Pandis,
319 2006, see eq. (S1-S3) in the supplement) is replaced by a water adsorption term. The
320 equations (1) and (2) show application of the Frenkel Halsey Hill adsorption isoterme
321 (FHH) as proposed by Sorjamaa and Laaksonen (2007) and Kumar et al. (2009):

322 $$B = -A_{FHH} \cdot \theta^{-B_{FHH}} \quad (1)$$

323 Therein the water coverage θ by (Sorjamaa and Laaksonen, 2007) is given as:

324 $$\theta = \frac{D_w - d_u}{2 \cdot 2.75 \cdot 10^{-4}} \quad [um] \quad (2)$$

325 and D_w and d_u are the diameter of the wet particles and the insoluble core. We applied
326 the FHH parameter for $CaCO_3$ (AFHH=0.25 and BFHH=1.19, Kumar et al. 2009) and
327 derived a critical supersaturation of 1.52% for $CaCO_3$ particles with d_u = 101.9 nm
328 (Figure 7, blue line). In comparison κ-Koehler theory predicts SS_{crit}=1.49% for
329 κ=0.0028. Such an SS_{crit}=1.49% would also be achieved by $8.5 \cdot 10^{-20}$ mole solute per
330 particle (Figure 7, black line). Figure 7 also shows the SS_{crit} for the bare CaCO3
331 particles processed at 80°C coating temperature and the range of SS_{crit} for 101.9nm

particles calculated from the range of κ's given in the literature (Tang et al., 2016 and references therein) for wet generated $CaCO_3$ particles.

We conclude that the surface of our $CaCO_3$ particles is a little more wettable than the dry generated particles studied by Kumar et al. (2009). We presume formation of $Ca(OH)(HCO_3)$ structures on the surface during the spray-drying generation process as commonly observed whenever the $CaCO_3$ surface has been exposed to gaseous water or liquid water (Stipp, 1999; Stipp and Hochella, 1991; Neagle and Rochester, 1990). In case of soluble components cauisng the lower SS_{crit} their amount must be of the order of $1 \cdot 10^{-19}$ mole per particles.

3.2 CCN activity of $CaCO_3$ particles with oleic acid coating

For the coating with oleic acid, we selected monodisperse $CaCO_3$ aerosol particles of 101.8 nm diameter using the DMA, and measured the size and chemical composition of the particles before (uncoated) and after (coated) coating with oleic acid. The results are listed in the upper part of Table 1.

The mode diameters of number size distribution for the uncoated $CaCO_3$ particles at 30-80 ºC remained in the 101.8 nm size bin, identical to that selected by the DMA. Interpolation in between the size bins as described in the experimental section led to an average dry diameters of bare $CaCO_3$ of d_u = 101.9 nm. The mode diameters of the $CaCO_3$ particles after coating with oleic acid in the range of 30-50 ºC stayed in the pre-selected size bin at 101.8 nm, which means that the layers were too thin to

effectively grow the particles to the next size bin; the mode diameters increased distinctively in the temperature range of 60-80 ºC (Fig. 3, upper panel). However, the bin-interpolated diameters D_P which are shown in Table 1 increased monotonically over the whole temperature range.

The values of *m/z*41 [µg per particle] originating from the oleic acid coating for the coated $CaCO_3$ particles at 30-80 ºC were at all temperatures significantly larger than for the bare $CaCO_3$ particles, and increased with the increasing coating temperature ($3.7 \cdot 10^{-12}$ - $390 \cdot 10^{-12}$ µg per particle, compare Table 1 and Fig. 3, bottom panel, red circles). The AMS detected increase at *m/z41* showed that the $CaCO_3$ particles already contained small amounts of oleic acid after coating with oleic acid at temperatures below 60 ºC although the D_P shifted less than a size bin.

The organic volume fraction (vf) in the aerosol particles, V_{OA}/V_{par} [%], was calculated. Herein $V_{par} = (V_{OA} + V_{CaCO3})$, V_{OA} is the oleic acid volume derived by AMS and V_{CaCO3} the volume of the bare $CaCO_3$ before coating (101.9 nm). V_{OA}/V_{par} for the uncoated $CaCO_3$ particles is by definition zero. The vf for the coated $CaCO_3$ particles at 30-80 ºC increased with the increase in the coating temperature from 0.8% at 30 ºC to 44% at 80 ºC (Fig. 3, bottom panel, red crosses and Table 1). The $CaCO_3$ particles were indeed coated with a significant amount of oleic acid and the amount of oleic acid coating increased with the increase in the coating temperature. The experiments were repeated at least four times. The according standard deviations for the oleic acid mass per particle in Table 1 demonstrate that the reproducibility of the experiments

was good and the performance of the coating device was stable.

The activated fractions at different SS for monodisperse $CaCO_3$ particles with d_u = 101.9 nm before and after oleic acid coating at 30-80 ºC are shown in Fig. 4. The top panel in Fig. 4 shows the results at 30-60 ºC with up to $23\pm1.2\cdot10^{-12}$ ug of coating material deposited on the $CaCO_3$ particles (vf = 4.3%). At the lowest SS of 0.17% and 0.35%, the activated fractions were very low and independent of the presence of the coating material within the errors. When the SS increased to 0.52%, 0.70%, and 0.87%, the activated fractions for the coated $CaCO_3$ particles were *lower* than those for the uncoated particles. Notably the activated fractions for the coated $CaCO_3$ particles *decreased* with the increase in the coating material in the range of vf 0.8-2.7%. The activated fractions for the $CaCO_3$ particles with different amounts of coating spread with larger SS applied. However this trend reversed at the coating temperature of 60 ºC and an oleic acid vf of 4.3%, and the activated fractions at vf = 4.3% became higher than those at 2.7% at the three largest SS. In summary, we found that the CCN activity of the coated $CaCO_3$ particles with vf of OA in a range 0.8-4.3% was lower than that of the uncoated $CaCO_3$ particles. The CCN activity of the coated $CaCO_3$ particles decreased with the increasing vf in between 0.8-2.7%, i.e. the CCN activity became lower when more coating material deposited on the $CaCO_3$ particles. This trend turned somewhere at a vf somewhere between 2.7 and 4.3%. As the D_P also increased at 60 ºC we cannot differentiate if the increase in the activated fractions is due to increasing size or because of increasing wettability.

394 The activated fractions of $CaCO_3$ particles after coating with oleic acid with vf of 16%
395 and 44% (coating temperatures of 70 and 80 ºC , respectively) were considerably
396 higher than that before coating, as shown in Fig. 4 (bottom panel). The increased
397 activated fractions resulted from both the increase in particle size (Fig. 3) and the
398 increase of the OA volume fraction of particles. At vf of 16% and 44%, the activated
399 fractions of the $CaCO_3$ particles after coating increased with the increase of SS and
400 reached complete activation. (Note, because the activation efficiency is 83%, the
401 activated fractions appear at values less than 100% at the points of full activation.)
402 For vf of 16% and 44% SS_{crit} was determined by fitting a sigmoidal function to the
403 activated fraction as a function of SS. The particle dry diameter D_P which is D_{crit} in
404 these cases is given as in Table 1. The hygoscopicity parameter κ was determined
405 from D_P (D_{crit}) and the corresponding SS_{crit}. The κ values of the $CaCO_3$ particles
406 coated with vf of oleic acid of 16% and 44% were 0.0237 ± 0.0006 and 0.0673 ±
407 0.0016, respectively. The respective κ values for the $CaCO_3$ particles with a diameter
408 of 101.9 nm without coating and after coating with oleic acid at 30-60 ºC (oleic acid
409 vf ≤4.1%) could not be determined by this method because these particles could not
410 be fully activated at the highest SS reachable by the CCN counter. Therefore we give
411 as upper limit $\kappa = 0.0028 \pm 0.0001$ for the uncoated $CaCO_3$ particles determined by
412 scanning the size of the poly-disperse $CaCO_3$ aerosol particles as described above (see
413 Fig. 5).

414 So we conclude that for vf of oleic acid of 0.8-2.7% the CCN activity of $CaCO_3$
415 particles after coating is lower than that of uncoated $CaCO_3$ particles and decreases

with the fraction of oleic acid. The trend turns at a vf between 2.7 and 4.3%. CCN activity was higher than that of the bare $CaCO_3$ particles at vf of oleic acid of 16% (70°C) and 44% (80°C) with CCN activity $\kappa = 0.0237 \pm 0.0006$ and $\kappa = 0.0673 \pm 0.0016$), respectively. The enhanced and reduced CCN activity of $CaCO_3$ particles coated with oleic acid at 80 ºC and 60 ºC, respectively, was also evident from the CCN activity measurement using *poly-disperse* aerosols (Fig. 5).

A possible explanation for our observation can be based on the amphiphilic character of oleic acid, namely that one end of the oleic acid molecule is hydrophobic (the hydrocarbon chain), while the other is hydrophilic (the carboxyl group).

We refer to $Ca(OH)(HCO_3)$ structures at the surface which offer polar surface sites to bind the hydrophilic ends (the carboxyl groups) of the oleic acid molecules. The hydrophobic ends of oleic acid molecules (the hydrocarbon chains) are then exposed on the particle surface hence increase the hydrophobicity of the particle surface. Such a formation of a hydrophobic layer should be occurring until all polar sites are occupied or monolayer coverage - maybe in form of a self-assembled layer - is reached. This can hinder the uptake of water. Activation of $CaCO_3$ particles can be described by the Kelvin term and a water absorption term, e.g. Frenkel Halsey Hill isotherm (Sorjamaa and Laaksonen, 2007, Kumar et al. 2009). In terms of Kelvin/FHH theory the hydrophobic OA coating will lower A_{FHH} and/or likely increase B_{FHH}. (The formation of a monolayer of OA on black carbon particles with the polar groups pointing outwards was postulated by Dalirian et al. (2017), which

lead to increased activation of the black carbon particles. Thus, they observed a similar effect of layer formation, but with switched polarity.)

Garland et al. (2008) suggested that OA at sub-monolayer coverage form self-associated islands rather than uniformly covering the surfaces, and OA molecules are oriented vertically, with polar heads facing to the surface. This is in support of our working hypothesis: the formation of a hydrophobic surface film. We conclude that all hygroscopic sides on the $CaCO_3$ surface are covered at OA vf somewhere between 2.7% and 4.3%, as here the trend turns and droplet activation starts to increase again. This would place the monolayer coverage above 3%, organic volume fraction. According to the measurements and calculations of the length of oleic acid molecule, the thickness of oleic acid sub-monolayer on solid surfaces, and the thickness of deuterated oleic acid monolayers at the air-water interface (Garland et al., 2008; King et at., 2009; Iwahashi et al., 2000), we estimate 2.3 nm as the likely thickness of oleic acid monolayer on $CaCO_3$ particles, accordingly a monolayer would be achieved at about 12-13% organic volume fraction. As a consequence the re-increase of hygroscopicity starts at sub-monolayer coverage and we propose that a fraction of oleic acid binds to already adsorbed oleic acid tail by tail such that carboxylic groups are facing outwards.

For $CaCO_3$ particles coated with more than an OA monolayer (vf = 16% and 44% at 70 and 80 ºC coating temperatures), OA in the first layer should still combine with the $CaCO_3$ surface, the heads pointing downwards. We suppose that now a portion of the

458 carboxyl groups of the oleic acid molecules, which are not in the first layer, will be
459 exposed to the particle surface, in analogy to the formation of lipid bilayers, e.g. in
460 cells, though the structure of this part of oleic acid is not known. The particle surface
461 then becomes more hydrophilic.

462 When carboxylic groups of OA are exposed at the surface, the interaction of water
463 with the OA layer becomes stronger, and the surface becomes wettable. In terms of
464 the Kelvin/FHH approach, the surface water interaction becomes stronger and A_{FHH}
465 increases and likely also the interaction between the higher water layers (B_{FHH}
466 decreases). From this point of view water adsorption by the "OA bilayer" should
467 become similar to thin malonic acid layers (compare next section). In addition, when
468 droplets form, oleic acid will transfer to the surface of the droplets and lower the
469 surface tension of the solution (the surface tension of oleic acid is 0.033 J m^{-2}, which
470 is much lower than that of pure water of 0.072 J m^{-2}). Thus, the activation of OA
471 coated particles is probably a complex interaction between formation of a specific
472 hydrophobic layers and more hydrophilic multilayers, surface tension effects and for
473 the largest coating amounts, simple size effects. As shown in Figure 7, SS_{crit} for OA is
474 lower than for thin malonic acid coatings, probably because of the surface tension
475 effect, but higher than for thick MA coatings, because of the missing solute effect.

476 The CCN activity of all oleic coated particles is higher than the CCN activity of pure
477 oleic acid. Our CCN activity measurement showed that pure oleic acid particles up to
478 333 nm did not activate at 0.87% SS; this sets an upper limit for CCN activity of oleic

acid particles ($\kappa < 0.0005$), in agreement with Kumar et al. (2003) and Broekhuizen et al. (2004). In liquid state oleic acid (OA) forms micelle like structures, the hydrophilic ends (the carboxyl groups) of oleic acid molecules tend to combine together by hydrogen bonds and the hydrophobic tails (the hydrocarbon chains) are exposed at the outside (Iwahashi et al., 2000; Garland et al., 2008). The arrangement of oleic acid molecules in pure oleic acid particles should be similar. Hydrophobic tails facing outwards can explain the hydrophobicity of the particle surface and the hindrance of the uptake of water, making the CCN activity of pure oleic acid particles very low. For sub-monolayer coatings of OA of vf 0.8 - 2.7% the CCN activity seem to approach that of pure OA. However, the arrangement of oleic acid molecules in these thin coatings will be influenced by the $CaCO_3$ core with its polar, hydrophilic sides differing from pure oleic acid particles and can thus be less hydrophobic

Even at the largest coating with an organic volume fraction of 44%, the coating thickness is about 10 nm, which corresponds to about only 4 monolayers of oleic acid (assuming the thickness of oleic acid monolayer on $CaCO_3$ particles is about 2.3 nm). And the arrangement of oleic acid molecules will still be likely influenced by the $CaCO_3$ core. Water can probably adsorb at the carboxylic groups facing outward ("bilayer" type structure) and diffuse through the thin oleic acid coatings. It may form an adsorbed water phase near the $CaCO_3$ surface. This could push the oleic acid out to act as surfactant which lowers the Kelvin term. Such processes should also happen in pure oleic acid particles. Because of the presence of $CaCO_3$ core the SS to achieve this is lower than for pure OA.

501 The phenomenon described above is reported for the first time in the studies on the
502 CCN activity of multicomponent aerosols. This phenomenon also shows a limitation
503 of the otherwise very useful mixing rule (Petters and Kreidenweis, 2007) for
504 multicomponent aerosols with specific morphologies.

505 In Fig. 5 we additionally show the influence of water vapor on CCN activity of
506 $CaCO_3$ particles coated with oleic acid for the highest coating temperature (80 °C)
507 and thus largest oleic acid amount. Herein we determined D_{crit} at different
508 super-saturations (SS_{crit}) for *poly-disperse* $CaCO_3$ aerosol particles (by SMCA). The
509 experiments were performed at RH 0.3% and at RH 3% at the coating temperature of
510 80 °C on cooling to room temperature the RH increased to 47%. The presence of
511 more water vapor (1500 Pa) in the coating process increased κ somewhat and
512 enhanced the CCN activity. This is of importance since often RH will larger than 0.3%
513 if coating appears in the atmosphere. This will be discussed further in context of
514 malonic acid coatings at enhanced water vapor.

515 **3.3 CCN activity of $CaCO_3$ particles with malonic acid coating**

516 For the study with malonic acid coatings, the $CaCO_3$ particles were also size selected
517 with a diameter of 101.8 nm. The size D_P and chemical composition of $CaCO_3$ aerosol
518 particles are listed in Table 1 before and after coating with malonic acid (MA) at
519 temperatures in a range of 30-80 ºC. The mode diameter did not shift after coating in a
520 temperature range of 30-60 ºC, but it increased for coatings at 70 and 80 ºC with
521 increasing coating temperature. The size bin interpolated particle diameter D_P of the

522 MA coated particles increased monotonically with the coating temperature. The
523 average of the interpolated diameter of bare $CaCO_3$ particles in the temperature range
524 30°C-80°C was d_u = 101.9 nm.

525 Values of the malonic acid marker *m/z*42 per particle were significantly larger for
526 $CaCO_3$ particles after coating at 30-80 ºC and the MA mass increased from $3.3 \cdot 10^{-12}$
527 to $610 \cdot 10^{-12}$ ug per particle with the coating temperature (Table 1, Figure 3, bottom
528 panel). The organic volume fraction vf of malonic acid ($V_{MA}/(V_{MA}+V_{CaCO3})$[%]) was
529 calculated as in the case of the oleic acid and ranged from 0.4 to 40%. As for oleic
530 acid the malonic acid experiments were repeated at least four times and the
531 reproducibility and stability were good (see standard deviations in Table 1).

532 The activated fractions at different SS for 101.9 nm $CaCO_3$ particles before and after
533 coating with malonic acid at 30-80 ºC are shown in Fig. 6. SS_{crit} was determined by
534 fitting a sigmoidal function to the data and the κ value was calculated from the
535 $D_P(D_{crit})$ and the corresponding SS_{crit}. The results are listed in Table 1. In this
536 procedure we had to neglect the contribution of double charged particles as the step in
537 the CN/CCN vs SS data in Fig.6 is not sufficiently expressed to separate a plateau for
538 multiply charged particles (e.g. Sullivan et al. 2009). The exception is the MA coating
539 with vf = 0.04%. For this case we compared a sigmoidal fitting both from the
540 beginning (the first point) and from the multiply-charged plateau (the third point) to
541 the "completely-activated plateau" (Figure S3, supplement). We yield SS_{crit} =
542 0.887±0.005% for fitting from the beginning and SS_{crit} = 0.900±0.013% for fitting

543 from the multiply-charged plateau, a difference of 0.013%. The underestimate in SS_{crit}
544 is the largest (0.013%) when the MA mass is the smallest (vf = 0.04%) and the
545 underestimate will be reduced with increasing vf of MA. At the largest two MA vf it
546 can be neglected. We have to concede a systematic error in SS_{crit}, but it is distinctively
547 less than 0.02%

548 The κ values of the $CaCO_3$ particles after coating with malonic acid at 30-80 ºC were
549 higher than the κ value of the uncoated $CaCO_3$ particles (κ = 0.0028 ± 0.0001), and
550 increased with the increasing coating MA mass per particle and increasing MA vf.
551 The CCN activity of the $CaCO_3$ particles increased monotonically after coating with
552 increasing malonic acid mass. This result differs from that of oleic acid which is not
553 surprising since malonic acid is easily soluble in water.

554 The κ value for the $CaCO_3$ particles after coating with a mass of malonic acid as small
555 as $3.3 \cdot 10^{-12}$ ug per particle and vf of MA of only 0.4% was 0.0123 ± 0.0005 thus
556 considerably larger than the κ value for the uncoated $CaCO_3$ particles (κ = 0.0028 ±
557 0.0001). This suggests that already a small amount of malonic acid can significantly
558 enhance the CCN activity of $CaCO_3$ particles. Such phenomenon, that traces of water
559 soluble substances can strongly affect droplet activation has been reported before
560 (Bilde and Svenningsson, 2004).

561 We applied Koehler theory to $CaCO_3$ particles coated with malonic acid assuming
562 that the malonic acid coating will fully dissolve in water when droplets form (see
563 supplement eq. (S1-S3). Increasing MA solute decreases the activity of water in

564 solution, and lowers the critical supersaturation SS_{crit} for droplet activation.

565 The resulting Koehler curves, i.e. equilibrium supersaturation (SS) over the solution
566 droplet as a function of the wet diameter D_w, are shown in Figure S2. Therein the
567 maximum of each SS curve is the critical supersaturation (theory SS_{crit}). In Table S1
568 and Figure 7 we compare the SS_{crit} predicted by the Köhler approach (red) with the
569 observed SS_{crit} (black). Koehler theory overpredicts SS_{crit} for thin coatings
570 substantially, meaning it underestimates the hygroscopicity of the thinly coated
571 particles. But with increasing coating Koehler theory approaches the observed SS_{crit}
572 and SS_{crit} for a particle of 121 nm diameter composed of pure malonic acid is the
573 limiting case (red circle).

574 From the Koehler results we derived the water content of the particles at SS_{crit} and we
575 calculated molality and mass fraction of the solute in the solution at the point of
576 activation. The molality at minimum and maximum malonic acid load of $3.3 \cdot 10^{-12}$
577 ug/particle and $610 \cdot 10^{-12}$ ug/particle were 0.006 mol kg^{-1} and 0.0015 mol kg^{-1},
578 respectively. We used these values in the AIOMFAC model (Zuend etal. 2011) to
579 calculate the deviation from ideality for the solution at point of activation for a flat
580 solution. The both solutions are highly non-ideal with respect to the MA (a_x = 0.4),
581 wherein MA was treated as solute with reference state infinite dilution (mole fraction
582 $x_{solute} \rightarrow 0$). However this did not affect much the activity coefficient of water, which
583 is essentially 1, water treated as solvent with reference state pure liquid (mole fraction
584 $x_{water} = 1$). Moreover, in this concentration range, the surface tension of aqueous

585 malonic acid solutions is about 0.070 J m^{-2}, thus the nearly same as for water (Table
586 S2 in the supplement). One should expect that Koehler theory would predict SS quite
587 well under such conditions.

588 To bring Köhler theory in agreement with the observation for the thinnest coating,
589 *more* solute entities would be required. Thus, disagreement cannot be caused by an ill
590 determined van't Hoff factor as we used already maximum $\nu = 3$ and reducing ν will
591 increase the deviation. Note, that recent observations point to the importance of the
592 surface effect by organic surface films over the solute effect for water soluble
593 inorganics in presence of organics, including malonic acid (Ruehl et al., 2016). A
594 lower surface tension will bring Koehler prediction and observation punctually in
595 better agreement and still allow for smaller van't Hoff factors. As an example, a
596 surface tension of 55% of σ_w and a van't Hoff factor of one will bring SS_{crit} predicted
597 by Koehler theory and observation in agreement for the thinnest coating. However, a
598 surface tension 55% of σ_w will cause disagreement for the thickest coating, because
599 the solute term gains in importance. Probably, the findings for the mixed solutions of
600 malonic acid and water soluble ammonium sulfate are not directly transferable to our
601 systems with insoluble inorganic core, where we expect dilute aqueous solutions of
602 0.006 mol/kg of malonic acid at the activation point. At such concentrations malonic
603 acid does not reduce σ_w, moreover in the study of Ruehl et al. (2016) malonic acid
604 was one of the more Koehler κ behaving organics.

605 In Figure 7 we show the prediction of SS_{crit}=1.52% for activating $CaCO_3$ by the

606 Kelvin/FHH theory with the $CaCO_3$ parameters taken from Kumar et al. (2009). SS_{crit}
607 for our bare $CaCO_3$ particles is 1.49% and the lower SS_{crit} should be due to a more
608 adsorptive surface, e.g. the presence of $Ca(OH)(HCO_3)$ structures. According to
609 classical Koehler theory the equivalent of $8.5 \cdot 10^{-20}$ moles of dissolvable entities
610 would be needed to explain a κ of 0.0028 and SS_{crit} of 1.49%, which is only about ¼
611 of the moles MA in the thinnest MA coating. Therefore, whatever makes our $CaCO_3$
612 particles wettable is not sufficient to explain the low SS_{crit} of 0.9 % at the thinnest MA
613 coating - in terms of Koehler theory.

614 We estimate monolayer coverage by MA at 2-3% vf; this would be achieved in
615 between MA mass loads of $13 \cdot 10^{-12}$ - $38 \cdot 10^{-12}$ ug per particle. Thus a sub-monolayer
616 coating of $3.3 \cdot 10^{-12}$ ug MA per particle caused a drop of SS_{crit} from 1.49 to 0.9 and
617 increased κ from 0.0028 to 0.012. Therefore we conclude that $CaCO_3$/MA coatings
618 show a non-Koehler behavior at thin coatings, but approach Koehler behavior with
619 increasing MA load.

620 This means there must be specific interactions between MA and the $CaCO_3$ surface
621 which eases water adsorption and CCN activation. We refer to the $Ca(OH)(HCO_3)$
622 structures that likely exist on the particle surface. When $CaCO_3$ particles are coated by
623 malonic acid (or oleic acid) the hydrophilic sides can serve as polar surface active
624 sites for accommodation of the acids. In case of MA there is no long hydrophobic
625 organic chain, but a second carboxylic group which still could support the adsorption
626 of water films.

627 In terms of Kelvin/FHH theory one could explain the observed low SS_{crit} for thin MA
628 coatings by net stronger interaction with water (higher A_{FHH}) and/or stronger
629 interaction between the adsorbed water layers (lower B_{FHH}) compared to bare $CaCO_3$.
630 If coatings become thicker the Koehler solute effect starts increasingly to contribute
631 and eventually controls the CCN activation. Our data are not sufficient to determine
632 A_{FHH} and B_{FHH}. (The only system in the literature which comes close - in a far sense -
633 is CaOxalate Monohydrate, with $A_{FHH} = 0.57$ of and $B_{FHH} = 0.88$ (Kumar et al., 2009).
634 Plugin in these FHH parameters will lead to $SS_{crit} = 0.53\%$ commensurable with our
635 observed value of 0.56% for $13 \cdot 10^{-12}$ ug MA coating which represents an organic
636 volume fraction of 1.6%, thus is close to monolayer.)

637 The D_{crit} at different super-saturations (SS_{crit}) for *poly-disperse* $CaCO_3$ aerosol
638 particles before and after coating with malonic acid are shown in Fig. 8. Our
639 observation of $\kappa = 0.25 \pm 0.04$ for pure malonic is consistent with the κ derived from
640 the data of Kumar et al. (2003) ($\kappa = 0.20$-0.25) and Prenni et al. (2001) ($\kappa = 0.24$), but
641 significantly lower than the κ derived from the data of Giebl et al. (2002) ($\kappa =$
642 0.41-1.04). The behavior of poly-disperse coated aerosol was similar to the result
643 obtained from the monodisperse $CaCO_3$ aerosol particles.

644 In Fig. 8 we added results for coating in presence of enhanced water vapor (1500 Pa)
645 and aerosols generated by spraying mixtures of malonic acid and $CaCO_3$. At the
646 coating temperature of 60 ºC, when the RH increased from 0.7% to 7% and eventually
647 to 47% at room temperature, the CCN activity of the coated $CaCO_3$ particles

increased substantially (compare "dry" (blue triangles) and "wet" (lilac triangles) in Fig. 8). The effect is more distinct than for the oleic acid coating shown in Fig. 5, and κ increases by about an order of magnitude. At a wet conditions, the reaction between $CaCO_3$ and malonic acid maybe more efficient and formation of calcium malonate will reduce d_u, i.e. the diameter of the insoluble core and according to eq, (S1) this may be the reason for the higher CCN activity at the higher RH. The hypothesis of malonate formation is supported by the CCN activity of "calcium malonate" aerosols, generated by spraying solutions containing $CaCO_3$ and malonic acid with molar ratios of about 1:1 and 3:1. Here the CCN activity is similar to that arising in the coating process in presence of water vapor. The change of the Ca/malonate ratio from 3:1 to 1:1 had no large effects. But taking the data of pure malonic acid particles also into account there is a trend to lower κ with increasing Ca in the initial solution.

The increasing of residence time (by 23.7 s) had no significant impact on CCN activity for both oleic acid coating and malonic acid coating at both dry and enhanced water vapor conditions, probably because the coating process was already completed in the coating device and no further reactions occurred in the flow tube.

Our findings may be important for aging processes of mineral particles in the atmosphere. The dependence of CCN activity of the coated particles on RH during the coating process will help to enhance the increase of the CCN activity by the coating process as water will be abundant in many instances. The effect probably will be relatively small for oleic acid and similar organics, which are hardly water soluble,

669 but strong for malonic acid and similar organic acids, which are highly water soluble.

670 4 Conclusions

671 The CCN activity of $CaCO_3$ particles with oleic acid and malonic acid coatings was
672 investigated in this study. The results show that oleic acid coating and malonic acid
673 coating have different impacts on the CCN activity of $CaCO_3$ particles. This can be
674 attributed to the amphiphilic property of oleic acid in contrast to the high water
675 solubility of malonic acid. Small amounts of oleic acid coating ($vf \leq 4.3\%$) decreased
676 the CCN activity of the $CaCO_3$ particles, while more oleic acid coating ($vf \geq 16\%$)
677 increased it. This phenomenon was reported here for the first time, and attributed to
678 stepwise passivating the active sites of $CaCO_3$ by oleic acid. Once all active sites are
679 occupied we suggest the formation of a lipid like bilayer with the carboxylic groups
680 facing outwards.

681 On the other hand, malonic acid coating (0.4-40%) increased the CCN activity of
682 $CaCO_3$ particles regardless of the amount of the coating. The CCN activity of $CaCO_3$
683 particles with malonic acid coating increased with the amount of the coating. Even a
684 small amount of malonic acid coating ($vf = 0.4\%$) significantly enhanced the CCN
685 activity of $CaCO_3$ particles from $\kappa = 0.0028 \pm 0.0001$ to $\kappa = 0.0123 \pm 0.0005$.
686 Increasing the relative humidity during the coating increased the CCN activity of the
687 $CaCO_3$ particles with malonic acid coating, probably because more $CaCO_3$ reacted
688 with malonic acid to soluble CaMalonate. This process will help to increase the CCN
689 activity.

690 Although malonic acid is well soluble in water, SS_{crit} for MA coated particles was
691 overpredicted by Köhler theory. Our results indicate that thin MA coatings provide a
692 wettable particle surface, which favors adsorption of water. For thicker coatings the
693 coated particles approached Köhler behavior, because of increasing importance of the
694 solute effect.

695 Mineral aerosol is one of the most abundant components of the atmospheric aerosol,
696 but its low water solubility limits its CCN activity. This study showed that
697 water-soluble organic acid coating might significantly enhance the CCN activity of
698 mineral aerosol particles. This could lead to mineral aerosol playing a more important
699 role in cloud formation.

700

701 **Acknowledgments**

702 This study was supported by Forschungszentrum Jülich, the National Natural Science
703 Foundation Committee of China (41421064, 21190051, 41121004), and the China
704 Scholarship Council.

705
706

References

AIOMFAC model, http://www.aiomfac.caltech.edu

Broekhuizen, K. E., Thornberry, T., Kumar, P. P., and Abbatt, J. P. D.: Formation of cloud condensation nuclei by oxidative processing: Unsaturated fatty acids, J. Geophys. Res.-Atmos., 109, D24206, 10.1029/2004jd005298, 2004.

Cakmur, R. V., Miller, R. L., Perlwitz, J., Geogdzhayev, I. V., Ginoux, P., Koch, D., Kohfeld, K. E., Tegen, I., and Zender, C. S.: Constraining the magnitude of the global dust cycle by minimizing the difference between a model and observations, J. Geophys. Res.-Atmos., 111, D06207, 10.1029/2005jd005791, 2006.

Charbouillot, T., Gorini, S., Voyard, G., Parazols, M., Brigante, M., Deguillaume, L., Delort, A. M., and Mailhot, G.: Mechanism of carboxylic acid photooxidation in atmospheric aqueous phase: Formation, fate and reactivity, Atmos. Environ., 56, 1-8, 10.1016/j.atmosenv.2012.03.079, 2012.

Chebbi, A. and P. Carlier (1996). "Carboxylic acids in the troposphere, occurrence, sources, and sinks: A review." Atmospheric Environment 30(24): 4233-4249.

Cheng, Y., Li, S. M., Leithead, A., Brickell, P. C., and Leaitch, W. R.: Characterizations of cis-pinonic acid and n-fatty acids on fine aerosols in the Lower Fraser Valley during Pacific 2001 Air Quality Study, Atmos. Environ., 38, 5789-5800, 10.1016/j.atmosenv.2004.01.051, 2004.

Chumpitaz, L. D. A., Coutinho, L. F., and Meirelles, A. J. A.: Surface tension of fatty acids and triglycerides, J. Am. Oil Chem. Soc., 76, 379-382, 10.1007/s11746-999-0245-6, 1999.

Cruz, C. N., and Pandis, S. N.: A study of the ability of pure secondary organic aerosol to act as cloud condensation nuclei, Atmos. Environ., 31, 2205-2214, 10.1016/s1352-2310(97)00054-x, 1997.

Dalirian, M., Ylisirniö, A., Buchholz, A., Schlesinger, D., Ström, J., Virtanen, A., and Riipinen, I.: Cloud droplet activation of black carbon particles coated with organic compounds of varying solubility, Atmos. Chem. Phys. Discuss., 2017, 1-25, 10.5194/acp-2017-1084, 2017.

DeCarlo, P. F., Kimmel, J. R., Trimborn, A., Northway, M. J., Jayne, J. T., Aiken, A. C., Gonin, M., Fuhrer, K., Horvath, T., Docherty, K. S., Worsnop, D. R., and Jimenez, J. L.: Field-deployable, high-resolution, time-of-flight aerosol mass spectrometer, Anal. Chem., 78, 8281-8289, 10.1021/ac061249n, 2006.

Falkovich, A. H., Ganor, E., Levin, Z., Formenti, P., and Rudich, Y.: Chemical and mineralogical analysis of individual mineral dust particles, J. Geophys. Res.-Atmos., 106, 18029-18036, 10.1029/2000jd900430, 2001.

Falkovich, A. H., Schkolnik, G., Ganor, E., and Rudich, Y.: Adsorption of organic compounds pertinent to urban environments onto mineral dust particles, J. Geophys. Res.-Atmos., 109, D02208, 10.1029/2003jd003919, 2004.

745 Gantt, B., Xu, J., Meskhidze, N., Zhang, Y., Nenes, A., Ghan, S. J., Liu, X., Easter, R., and
746 Zaveri, R.: Global distribution and climate forcing of marine organic aerosol - Part 2: Effects
747 on cloud properties and radiative forcing, Atmos. Chem. Phys., 12, 6555-6563,
748 10.5194/acp-12-6555-2012, 2012.

749 Garimella, S., Huang, Y. W., Seewald, J. S., and Cziczo, D. J.: Cloud condensation nucleus
750 activity comparison of dry- and wet-generated mineral dust aerosol: the significance of
751 soluble material, Atmos. Chem. Phys., 14, 6003-6019, 10.5194/acp-14-6003-2014, 2014.

752 Garland, E. R., Rosen, E. P., Clarke, L. I., and Baer, T.: Structure of submonolayer oleic acid
753 coverages on inorganic aerosol particles: evidence of island formation, Phys. Chem. Chem.
754 Phys., 10, 3156-3161, 10.1039/b718013f, 2008.

755 Giebl, H., Berner, A., Reischl, G., Puxbaum, H., Kasper-Giebl, A., and Hitzenberger, R.:
756 CCN activation of oxalic and malonic acid test aerosols with the University of Vienna cloud
757 condensation nuclei counter, J. Aerosol Sci., 33, 1623-1634, Pii s0021-8502(02)00115-5,
758 10.1016/s0021-8502(02)00115-5, 2002.

759 Gierlus, K. M., Laskina, O., Abernathy, T. L., and Grassian, V. H.: Laboratory study of the
760 effect of oxalic acid on the cloud condensation nuclei activity of mineral dust aerosol, Atmos.
761 Environ., 46, 125-130, 10.1016/j.atmosenv.2011.10.027, 2012.

762 Hartz, K. E. H., Tischuk, J. E., Chan, M. N., Chan, C. K., Donahue, N. M., and Pandis, S. N.:
763 Cloud condensation nuclei activation of limited solubility organic aerosol, Atmos. Environ.,
764 40, 605-617, 10.1016/j.atmosenv.2005.09.076, 2006.

765 Hatch, C. D., Gierlus, K. M., Schuttlefield, J. D., and Grassian, V. H.: Water adsorption and
766 cloud condensation nuclei activity of calcite and calcite coated with model humic and fulvic
767 acids, Atmos. Environ., 42, 5672-5684, 10.1016/j.atmosenv.2008.03.005, 2008.

768 Haywood, J., and Boucher, O.: Estimates of the direct and indirect radiative forcing due to
769 tropospheric aerosols: A review, Reviews of Geophysics, 38, 513-543,
770 10.1029/1999rg000078, 2000.

771 Herich, H., Tritscher, T., Wiacek, A., Gysel, M., Weingartner, E., Lohmann, U.,
772 Baltensperger, U., and Cziczo, D. J.: Water uptake of clay and desert dust aerosol particles at
773 sub- and supersaturated water vapor conditions, Phys. Chem. Chem. Phys., 11, 7804-7809,
774 10.1039/b901585j, 2009.

775 Ho, K. F., Cao, J. J., Lee, S. C., Kawamura, K., Zhang, R. J., Chow, J. C., and Watson, J. G.:
776 Dicarboxylic acids, ketocarboxylic acids, and dicarbonyls in the urban atmosphere of China,
777 J. Geophys. Res.-Atmos., 112, D22s27, 10.1029/2006jd008011, 2007.

778 Ho, K. F., Lee, S. C., Ho, S. S. H., Kawamura, K., Tachibana, E., Cheng, Y., and Zhu, T.:
779 Dicarboxylic acids, ketocarboxylic acids, alpha-dicarbonyls, fatty acids, and benzoic acid in
780 urban aerosols collected during the 2006 Campaign of Air Quality Research in Beijing
781 (CAREBeijing-2006), J. Geophys. Res.-Atmos., 115, D19312, 10.1029/2009jd013304, 2010.

782 Hori, M., Ohta, S., Murao, N., and Yamagata, S.: Activation capability of water soluble
783 organic substances as CCN, J. Aerosol Sci., 34, 419-448, 10.1016/s0021-8502(02)00190-8,

784 2003.

785 Iwahashi, M., Kasahara, Y., Matsuzawa, H., Yagi, K., Nomura, K., Terauchi, H., Ozaki, Y.,
786 and Suzuki, M.: Self-diffusion, dynamical molecular conformation, and liquid structures of
787 n-saturated and unsaturated fatty acids, J. Phys. Chem. B, 104, 6186-6194,
788 10.1021/jp000610l, 2000.

789 Kawamura, K., and Ikushima, K.: Seasonal-changes in the distribution of dicarboxylic-acids
790 in the urban atmosphere, Environ. Sci. Technol., 27, 2227-2235, 10.1021/es00047a033, 1993.

791 Kawamura, K., Kasukabe, H., and Barrie, L. A.: Source and reaction pathways of
792 dicarboxylic acids, ketoacids and dicarbonyls in arctic aerosols: One year of observations,
793 Atmos. Environ., 30, 1709-1722, 10.1016/1352-2310(95)00395-9, 1996.

794 Kawamura, K., and Bikkina, S.: A review of dicarboxylic acids and related compounds in
795 atmospheric aerosols: Molecular distributions, sources and transformation, Atmospheric
796 Research, 170, 140-160, 10.1016/j.atmosres.2015.11.018, 2016.

797 Keiser, E. H., and Leavitt, S.: On the preparation and the composition of the acid carbonates
798 of calcium and barium, J. Am. Chem. Soc. , 30, 1711-1714, 10.1021/ja01953a008, 1908.

799 Khare, P., et al. (1999). "Atmospheric formic and acetic acids: An overview." Reviews of
800 Geophysics 37(2): 227-248.

801 King, M. D., Rennie, A. R., Thompson, K. C., Fisher, F. N., Dong, C. C., Thomas, R. K.,
802 Pfrang, C., and Hughes, A. V.: Oxidation of oleic acid at the air-water interface and its
803 potential effects on cloud critical supersaturations, Phys. Chem. Chem. Phys., 11, 7699-7707,
804 10.1039/b906517b, 2009.

805 Koehler, H.: The nucleus in and the growth of hygroscopic droplets, Trans. Faraday Soc., 32,
806 1152-1161, 10.1039/tf9363201152, 1936.

807 Koehler, K. A., Kreidenweis, S. M., DeMott, P. J., Petters, M. D., Prenni, A. J., and Carrico,
808 C. M.: Hygroscopicity and cloud droplet activation of mineral dust aerosol, Geophys. Res.
809 Lett., 36, L08805, 10.1029/2009gl037348, 2009.Kumar, P. P., Broekhuizen, K., and Abbatt,
810 J. P. D.: Organic acids as cloud condensation nuclei: Laboratory studies of highly soluble and
811 insoluble species, Atmos. Chem. Phys., 3, 509-520, 2003.

812 Kumar, P. P., Broekhuizen, K., and Abbatt, J. P. D.: Organic acids as cloud condensation
813 nuclei: Laboratory studies of highly soluble and insoluble species, Atmos. Chem. Phys., 3,
814 509-520, 2003.

815 Kumar, P., Nenes, A., and Sokolik, I. N.: Importance of adsorption for CCN activity and
816 hygroscopic properties of mineral dust aerosol, Geophys. Res. Lett., 36,
817 10.1029/2009gl040827, 2009.

818 Li, W. J., and Shao, L. Y.: Mixing and water-soluble characteristics of particulate organic
819 compounds in individual urban aerosol particles, J. Geophys. Res.-Atmos., 115, D02301,
820 10.1029/2009jd012575, 2010.

821 Liu, X. H., and Wang, J. A.: How important is organic aerosol hygroscopicity to aerosol

indirect forcing?, Environ. Res. Lett., 5, 044010, 10.1088/1748-9326/5/4/044010, 2010.

Mkoma, S. L., and Kawamura, K.: Molecular composition of dicarboxylic acids, ketocarboxylic acids, alpha-dicarbonyls and fatty acids in atmospheric aerosols from Tanzania, East Africa during wet and dry seasons, Atmos. Chem. Phys., 13, 2235-2251, 10.5194/acp-13-2235-2013, 2013.

Moore, R. H., Nenes, A., and Medina, J.: Scanning Mobility CCN Analysis-A Method for Fast Measurements of Size-Resolved CCN Distributions and Activation Kinetics, Aerosol Sci. Technol., 44, 861-871, 10.1080/02786826.2010.498715, 2010.

Neagle, W., and Rochester, C. H., Infrared study of the adsorption of water and ammonia on calcium carbonate. Journal of the Chemical Society, Faraday Transactions, 86, 181-183, 1990.

Penner, J. E., Dong, X. Q., and Chen, Y.: Observational evidence of a change in radiative forcing due to the indirect aerosol effect, Nature, 427, 231-234, 10.1038/nature02234, 2004.

Petters, M. D., and Kreidenweis, S. M.: A single parameter representation of hygroscopic growth and cloud condensation nucleus activity, Atmos. Chem. Phys., 7, 1961-1971, 2007.

Rogge, W. F., Hildemann, L. M., Mazurek, M. A., Cass, G. R., and Simoneit, B. R. T.: Sources of fine organic aerosol .2. Noncatalyst and catalyst-equipped automobiles and heavy-duty diesel trucks, Environ. Sci. Technol., 27, 636-651, 10.1021/es00041a007, 1993.

Rogge, W. F., Hildemann, L. M., Mazurek, M. A., Cass, G. R., and Simoneit, B. R. T.: Sources of fine organic aerosol. 9. Pine, oak and synthetic log combustion in residential fireplaces, Environ. Sci. Technol., 32, 13-22, 10.1021/es960930b, 1998.

Rose, D., Gunthe, S. S., Mikhailov, E., Frank, G. P., Dusek, U., Andreae, M. O., and Poschl, U.: Calibration and measurement uncertainties of a continuous-flow cloud condensation nuclei counter (DMT-CCNC): CCN activation of ammonium sulfate and sodium chloride aerosol particles in theory and experiment, Atmos. Chem. Phys., 8, 1153-1179, 2008.

Ruehl, C. R., Davies, J. F., and Wilson, K. R.: An interfacial mechanism for cloud droplet formation on organic aerosols, Science, 351, 1447-1450, 10.1126/science.aad4889, 2016.

Russell, L. M., Maria, S. F., and Myneni, S. C. B.: Mapping organic coatings on atmospheric particles, Geophys. Res. Lett., 29, 1779, 10.1029/2002gl014874, 2002.

Sage, A. M., Weitkamp, E. A., Robinson, A. L., and Donahue, N. M.: Reactivity of oleic acid in organic particles: changes in oxidant uptake and reaction stoichiometry with particle oxidation, Phys. Chem. Chem. Phys., 11, 7951-7962, 10.1039/b904285g, 2009.

Schauer, J. J., Kleeman, M. J., Cass, G. R., and Simoneit, B. R. T.: Measurement of emissions from air pollution sources. 1. C-1 through C-29 organic compounds from meat charbroiling, Environ. Sci. Technol., 33, 1566-1577, 10.1021/es980076j, 1999.

Sorjamaa, R., and Laaksonen, A.: The effect of H₂O adsorption on cloud drop activation of insoluble particles: a theoretical framework, Atmos. Chem. Phys., 7, 6175-6180, 10.5194/acp-7-6175-2007, 2007.

Stipp, S. L. S.: Toward a conceptual model of the calcite surface: hydration, hydrolysis, and surface potential. Geochimica et Cosmochimica Acta, 63, 3121-3131, 1999.

Stipp, S. L., Hochella Jr, M. F.: Structure and bonding environments at the calcite surface as observed with X-ray photoelectron spectroscopy (XPS) and low energy electron diffraction (LEED). Geochimica et Cosmochimica Acta, 55, 1723-1736,1991.

Sullivan, R. C., Moore, M. J. K., Petters, M. D., Kreidenweis, S. M., Roberts, G. C., and Prather, K. A.: Effect of chemical mixing state on the hygroscopicity and cloud nucleation properties of calcium mineral dust particles, Atmos. Chem. Phys., 9, 3303-3316, 10.5194/acp-9-3303-2009, 2009.

Sullivan, R. C., Moore, M. J. K., Petters, M. D., Kreidenweis, S. M., Qafoku, O., Laskin, A., Roberts, G. C., and Prather, K. A.: Impact of Particle Generation Method on the Apparent Hygroscopicity of Insoluble Mineral Particles, Aerosol Sci. Technol., 44, 830-846, 10.1080/02786826.2010.497514, 2010.

Takegawa, N., Miyakawa, T., Kawamura, K., and Kondo, Y.: Contribution of selected dicarboxylic and omega-oxocarboxylic acids in ambient aerosol to the m/z 44 signal of an aerodyne aerosol mass spectrometer, Aerosol Sci. Technol., 41, 418-437, 10.1080/02786820701203215, 2007.

Tang, M. J., Cziczo, D. J., and Grassian, V. H.: Interactions of Water with Mineral Dust Aerosol: Water Adsorption, Hygroscopicity, Cloud Condensation, and Ice Nucleation, Chemical Reviews, 116, 4205-4259, 10.1021/acs.chemrev.5b00529, 2016.

Tang, M. J., Whitehead, J., Davidson, N. M., Pope, F. D., Alfarra, M. R., McFiggans, G., and Kalberer, M.: Cloud condensation nucleation activities of calcium carbonate and its atmospheric ageing products, Phys. Chem. Chem. Phys., 17, 32194-32203, 10.1039/c5cp03795f, 2015.

Yamashita, K., Murakami, M., Hashimoto, A., and Tajiri, T.: CCN Ability of Asian Mineral Dust Particles and Their Effects on Cloud Droplet Formation, Journal of the Meteorological Society of Japan, 89, 581-587, 10.2151/jmsj.2011-512, 2011.

Zhao, D. F., Buchholz, A., Mentel, T. F., Muller, K. P., Borchardt, J., Kiendler-Scharr, A., Spindler, C., Tillmann, R., Trimborn, A., Zhu, T., and Wahner, A.: Novel method of generation of Ca(HCO(3))(2) and CaCO(3) aerosols and first determination of hygroscopic and cloud condensation nuclei activation properties, Atmos. Chem. Phys., 10, 8601-8616, 10.5194/acp-10-8601-2010, 2010.

Zuend, A., Marcolli, C., Booth, A. M., Lienhard, D. M., Soonsin, V., Krieger, U. K., Topping, D. O., McFiggans, G., Peter, T., and Seinfeld, J. H.: New and extended parameterization of the thermodynamic model AIOMFAC: calculation of activity coefficients for organic-inorganic mixtures containing carboxyl, hydroxyl, carbonyl, ether, ester, alkenyl, alkyl, and aromatic functional groups, Atmospheric Chemistry and Physics, 11, 9155-9206, 10.5194/acp-11-9155-2011, 2011.

Table 1. Mode diameters, chemical compositions, and κ values of $CaCO_3$ aerosol particles (size selected by DMA at 101.8 nm) before (uncoated) and after coating with oleic (OA) or malonic acid (MA) at 30-80 ºC.

	D_P [nm]	Organic mass per particle [10^{-12}µg]	Mole organics per particle [10^{-20} mole]	Org. volume fraction [%]	κ
Oleic acid					
Uncoated $CaCO_3$ 30-80 ºC	101.9	(backgr. *m/z*41: 2.7±0.9)	0	0.0	0.0028±0.0001
$CaCO_3$+Oleic acid 30 ºC	102.1	3.7±1.9	1.3	0.8	
$CaCO_3$+Oleic acid 40 ºC	102.5	7.0±2.8	2.5	1.4	
$CaCO_3$+Oleic acid 50 ºC	103.7	14±3.7	5.1	2.7	
$CaCO_3$+Oleic acid 60 ºC	104.9	23±1.2	8.3	4.3	
$CaCO_3$+Oleic acid 70 ºC	109.2	96±3.7	34	16	0.0241±0.0006
$CaCO_3$+Oleic acid 80 ºC	123.7	390±14	140	44	0.0649±0.0008
Malonic acid					
Uncoated $CaCO_3$ 30-80 ºC	101.9	(backgr. *m/z*42: 1.4±0.4)	0	0.0	0.0028±0.0001
$CaCO_3$+Malonic acid 30 ºC	102.0	3.3±0.3	3.2	0.4	0.0123±0.0005
$CaCO_3$+Malonic acid 40 ºC	102.1	6.8±1.2	6.5	0.8	0.0231±0.0008
$CaCO_3$+Malonic acid 50 ºC	102.2	13±1.8	13	1.5	0.0380±0.0012
$CaCO_3$+Malonic acid 60 ºC	102.7	38±1.6	36	4.1	0.1063±0.0023
$CaCO_3$+Malonic acid 70 ºC	107.8	160±8.1	160	15	0.1907±0.0031
$CaCO_3$+Malonic acid 80 ºC	121.0	610±24	590	40	0.3126±0.0062

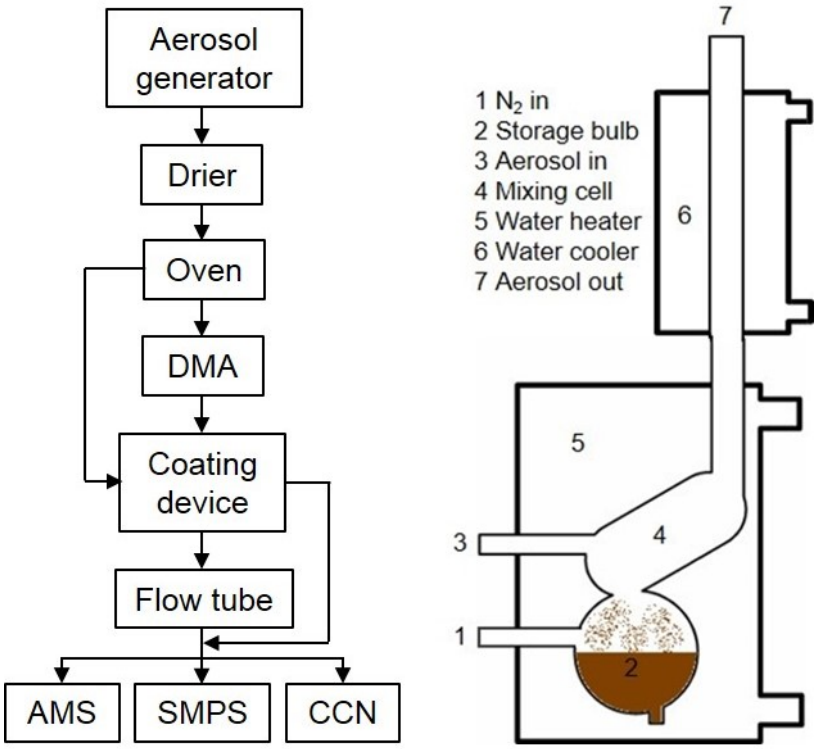

Figure 1. Schematics of the experimental set up (left side). $CaCO_3$ aerosol is generated by spray-drying of saturated $Ca(HCO_3)_2$ solutions and tempering the aerosol passing through an oven at 300°C. The *poly-disperse* $CaCO_3$ aerosol is either led directly to the coating device (right side, after Roselli, 2006) or led to a differential mobility Analyzer (DMA) for size selection first. Optional, a flow tube can be switched into the pass to enhance the reaction time of the coated particles. The stream of coated particles is finally split to the analytical instruments, namely aerosol mass spectrometer (AMS), scanning mobility particle sizer (SMPS) and CCN counter.

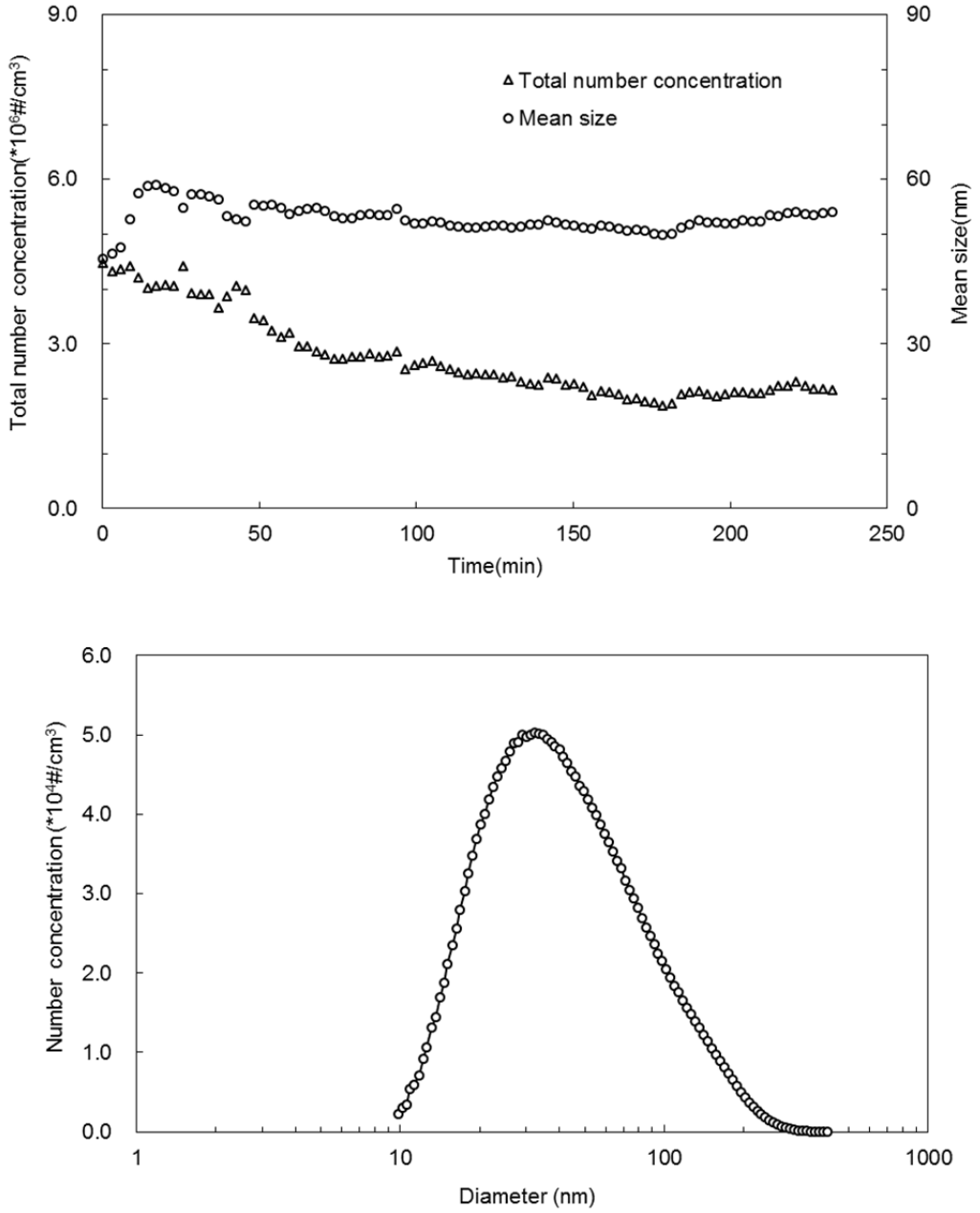

Figure 2. Total number concentration and mean diameter of $CaCO_3$ aerosol particles generated as a function of the spraying time (upper panel). Typical size distribution of the $CaCO_3$ aerosol after 70 min spraying (lower panel).

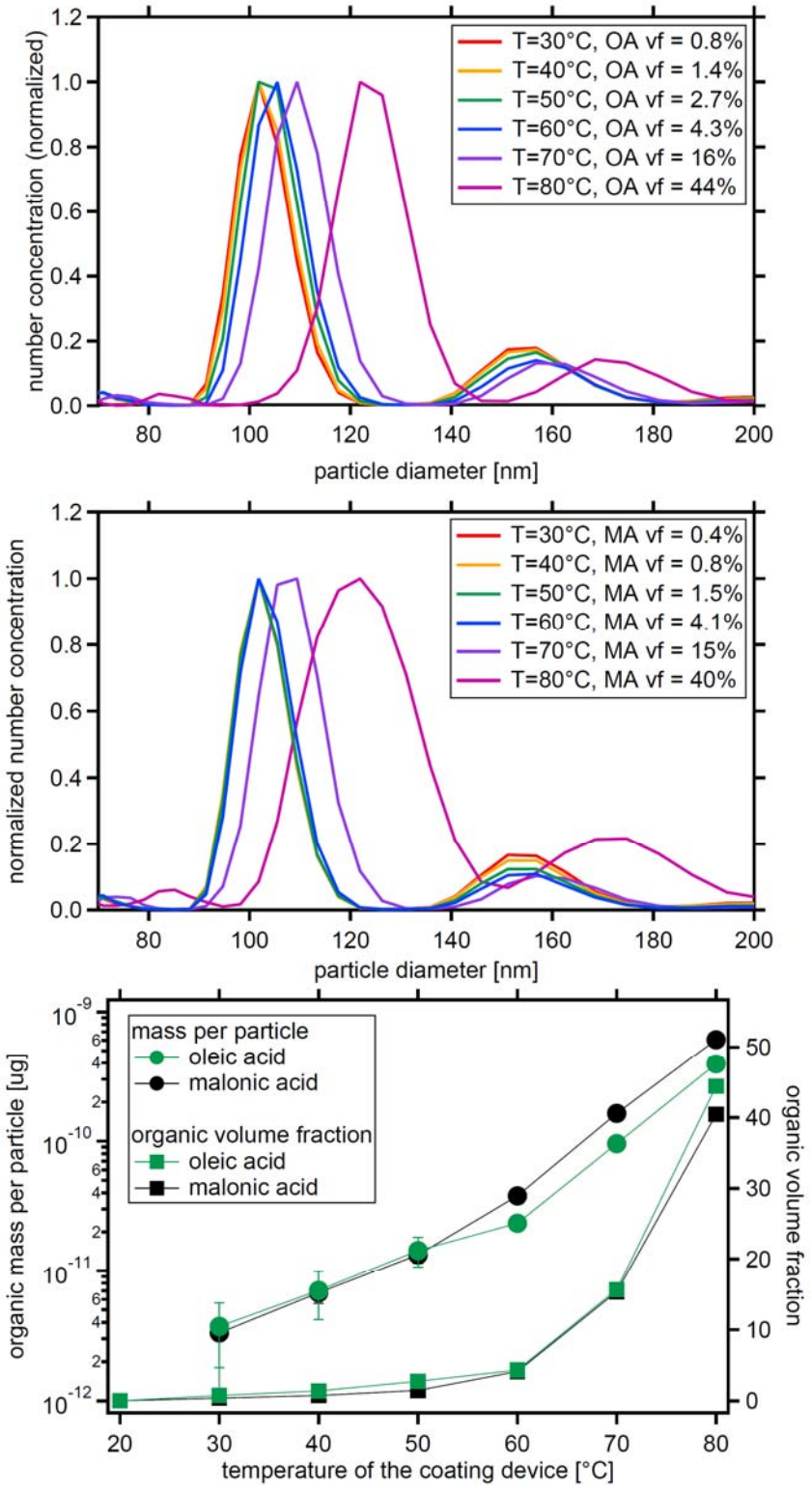

Figure 3. Size distribution of monodisperse $CaCO_3$ aerosol particles after coating with oleic acid (top panel) or malonic acid (middle panel). Coating amount and organic volume fraction for oleic and malonic acid as a function of the coating temperature for the same experiments (bottom panel, data in Table 1).

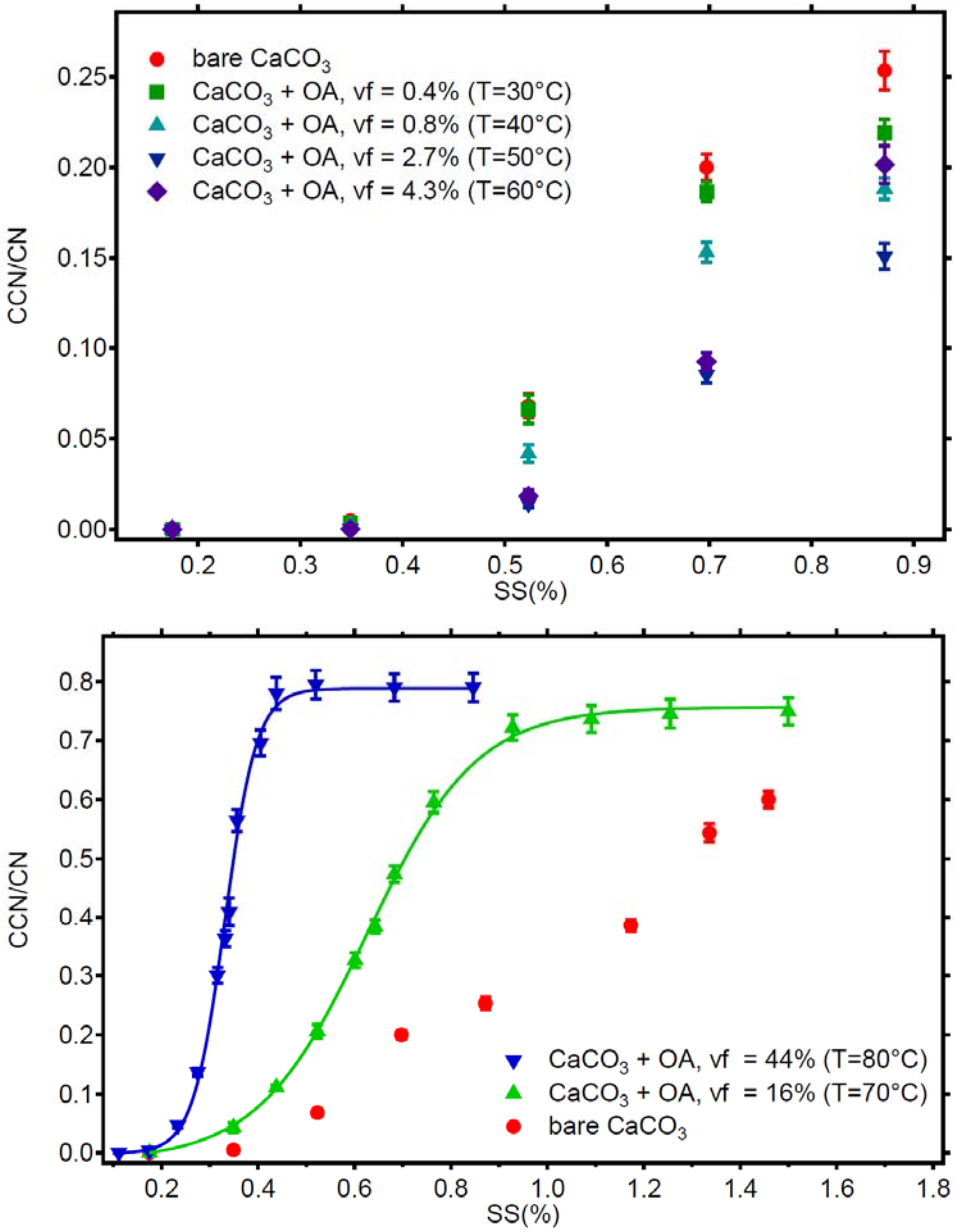

Figure 4. Activated fractions (CCN/CN) of *monodisperse* $CaCO_3$ aerosol particles (diameter d_u = 101.9 nm) at different supersaturations before and after oleic acid coating. With increasing coating temperatures of 30-50 ºC the activated fraction decreases despite the increase of organic vf from 0.8% - 2.7%. At vf = 4.3% at 60°C this trend turns. Considering the invariant particle diameter at 30-50 ºC, the increased particle diameter at 60 ºC, and the reduced activated fraction simultaneously, the CCN activity of the coated $CaCO_3$ particles at 30-60 ºC was lower than that of the uncoated $CaCO_3$ particles (top panel). At coating vf of 16% and 44% (T= 70-80 ºC) the activated fractions, thus CCN activities, are higher than for bare $CaCO_3$ and increase with coating vf. In these two cases all particles are activated at the highest SS and SS_{crit} and κ can be determined from the turning point of the sigmoidal fit (bottom panel, compare Table 1).

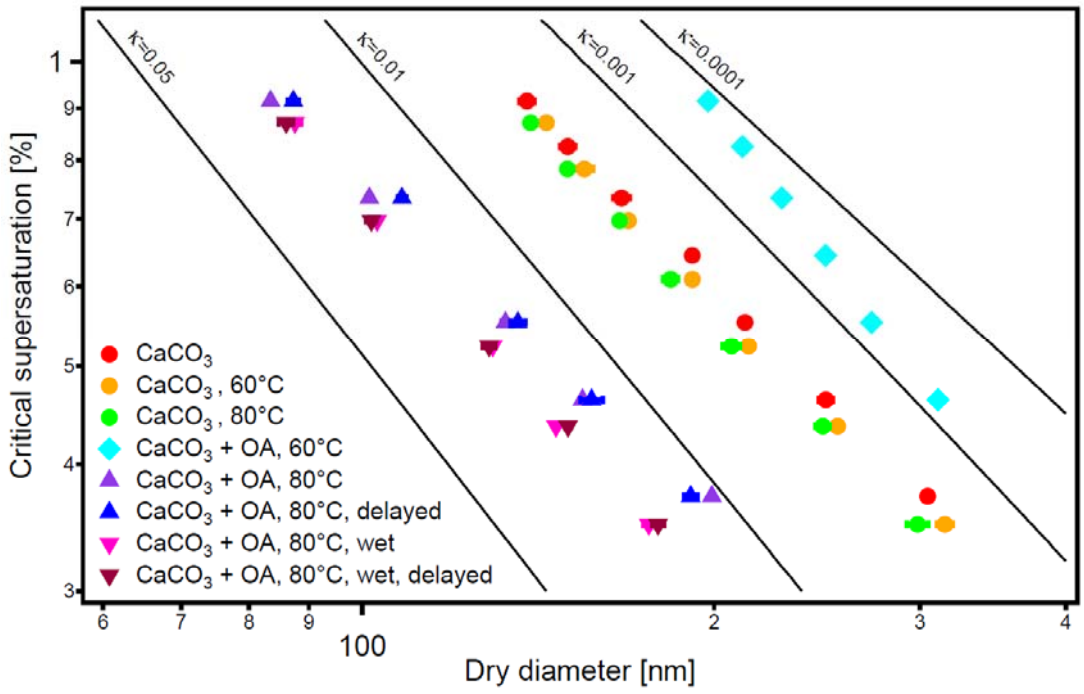

Figure 5. Critical dry diameters at different supersaturations (SS) of *poly-disperse* $CaCO_3$ aerosol before (circles) and after oleic acid coating. Experiments were performed at 60°C (turquoise diamond) and 80°C (triangles) coating temperatures. The flow tube experiments at 80° C were performed (indicated by 'delayed') at dry conditions (normal, blue tringles) and at enhanced water vapor ('wet', brown triangles). The effect of the temperature in the coating device on the $CaCO_3$ core is negligible (red, green, and orange circles). As for the monodisperse case in Figure 4, at 60° coating temperature the particles are less CCN active than bare $CaCO_3$ while at 80°C the coated particle more CCN active. The presence of water vapor (1500 Pa) in the coating process enhances CCN activity. The increasing of residence time (23.7 s) of the coated aerosol in the flow tube had no significant effect on CCN activity in both experiments.

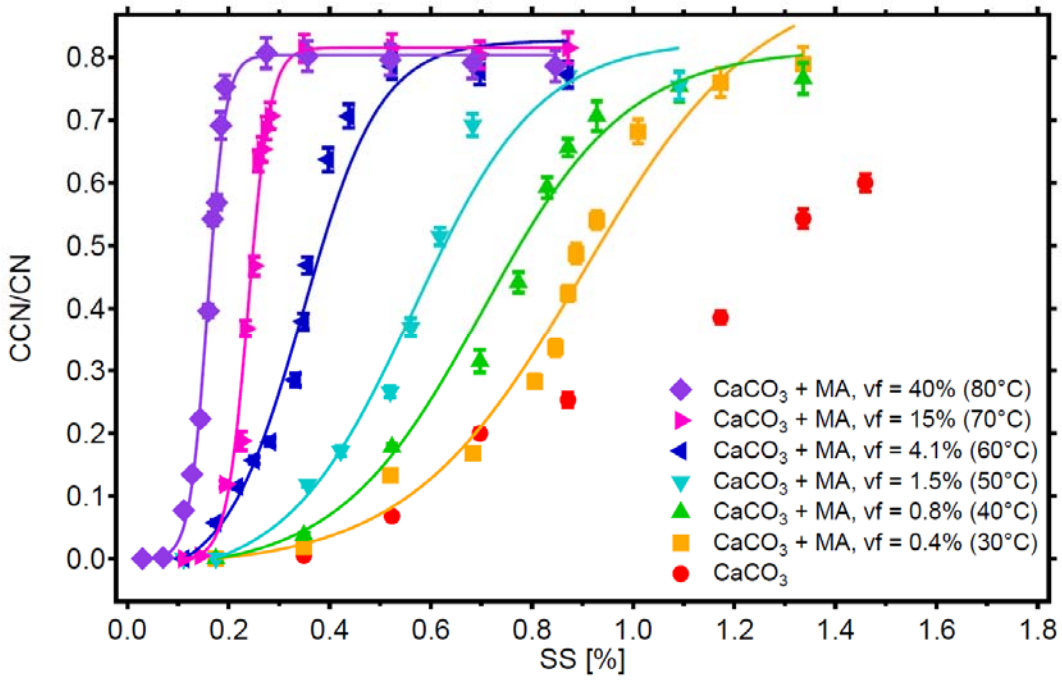

Figure 6. Activated fractions (CCN/CN) of *monodisperse* $CaCO_3$ aerosol particles (with $CaCO_3$ core, d_u = 101.9 nm) at different supersaturations before (red circles) and after malonic acid coating. With increasing coating, i.e. MA volume fraction vf the activated fraction, thus CCN activity, increase compared to bare $CaCO_3$ particles. All coated particles can be activated at sufficiently high SS and SS_{crit} and κ was determined (see Table 1).

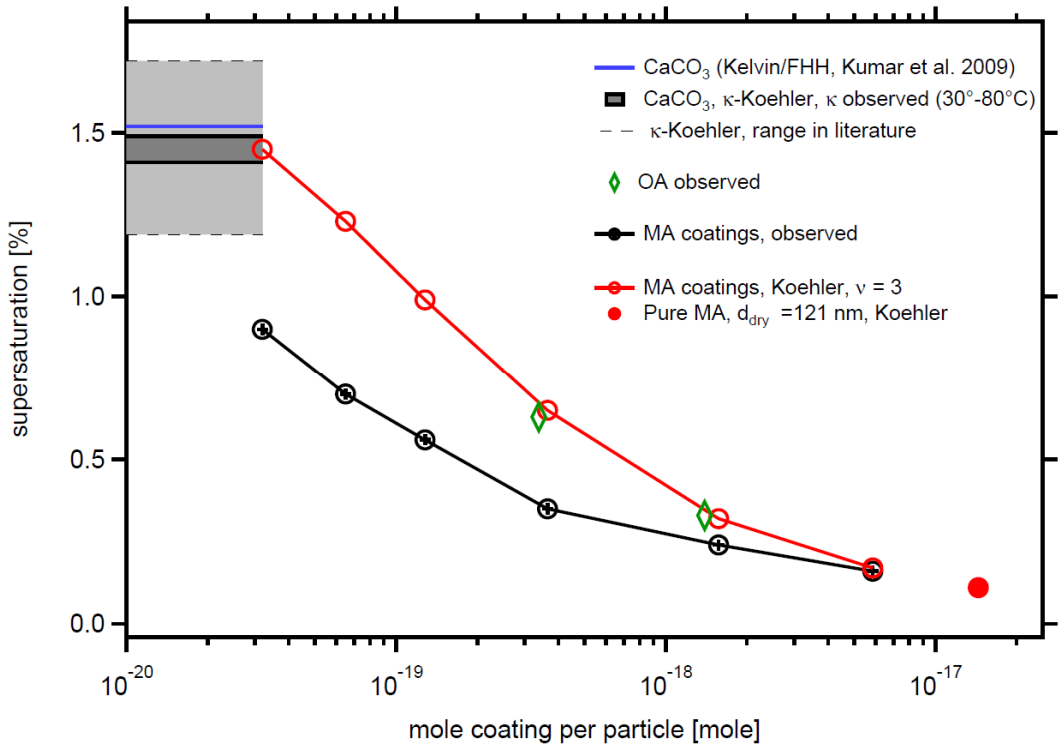

Figure 7: Comparison of SS_{crit} predicted by Koehler theory with observations. Koehler theory for aqueous MA solutions assuming full dissociation overpredicts SS_{crit} (red circles) compared to the observation (black circles). With increasing coating amount Koehler theory approaches the observation, with the limiting SS_{crit} for 121.0 nm particles made of pure malonic acid.
For comparison we show observed SS_{crit} for the two thickest OA coatings (diamonds show).
The horizontal lines indicate SS_{crit} of the bare $CaCO_3$ particles as calculated from our observed κ observed (black) and predicted by Kelvin/FFH theory (blue). Light grey area between the thin dashed grey lines shows the range of SS_{crit} for 101.9 nm particles calculated from the range of κ in literature for wet generated $CaCO_3$ particles (compare Tang et al. 2016).

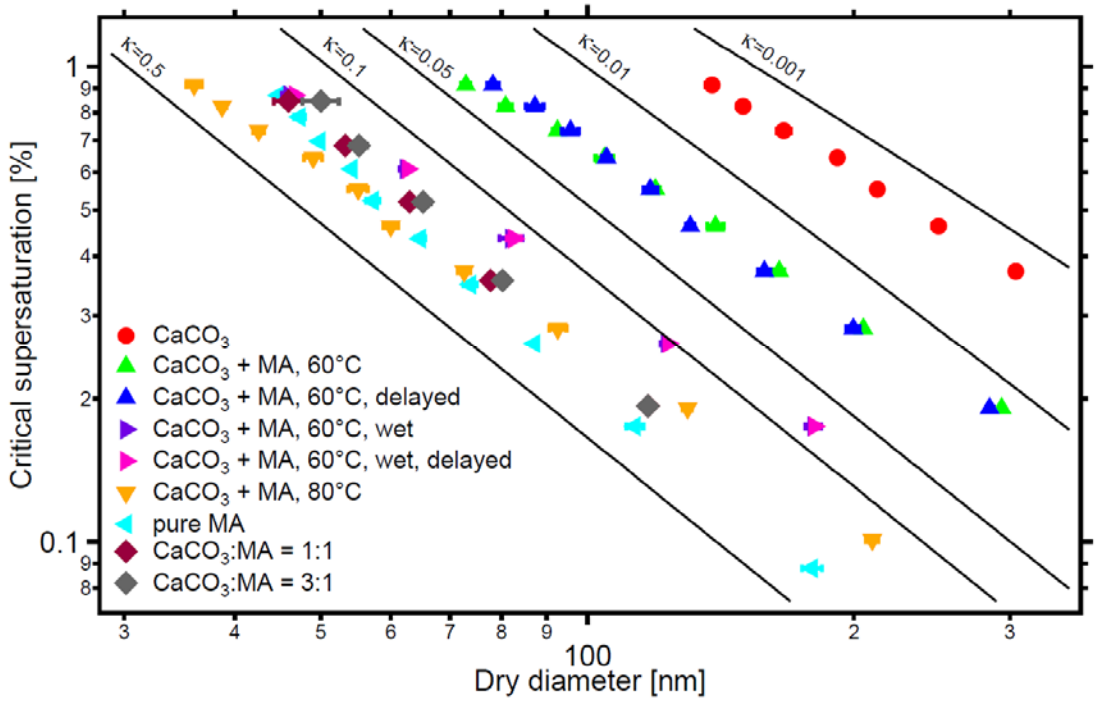

Figure 8. Critical dry diameters at different super-saturations (SS) of *poly-disperse* $CaCO_3$ aerosol before (circles) and after malonic acid coating (triangles). Experiments were performed at 60°C and 80°C coating temperatures. The results are similar to the monodisperse case in Figure 6. Critical dry diameters as a function of SS are also shown for malonic acid particles and particles that were generated by spraying mixed solution with molar ratios of $CaCO_3$/malonic acid of 1:1 and 3:1. The CCN activity decreases with increasing $CaCO_3$ content. The flow tube experiments at 60 °C were performed (indicated by 'delayed') at dry condition (blue tringles) and in presence of 1500 Pa water vapor (magenta triangles). The presence of water in the coating process substantially enhanced κ and CCN activity. The increasing of residence time (23.7 s) of the coated aerosol in the flow tube had no significant effect on CCN activity in both experiments.